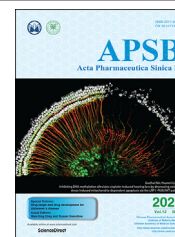




Chinese Pharmaceutical Association
Institute of Materia Medica, Chinese Academy of Medical Sciences

Acta Pharmaceutica Sinica B

www.elsevier.com/locate/apsb
www.sciencedirect.com



ORIGINAL ARTICLE

The upregulated intestinal folate transporters direct the uptake of ligand-modified nanoparticles for enhanced oral insulin delivery



Jingyi Li^{a,b}, Yaqi Zhang^{b,c}, Miaorong Yu^b, Aohua Wang^{b,c}, Yu Qiu^{b,c},
Weiwei Fan^b, Lars Hovgaard^d, Mingshi Yang^e, Yiming Li^a,
Rui Wang^{a,*}, Xiuying Li^{f,*}, Yong Gan^{b,c,g,*}

^aSchool of Pharmacy, Shanghai University of Traditional Chinese Medicine, Shanghai 201203, China

^bState Key Laboratory of Drug Research, Shanghai Institute of Materia Medica, Chinese Academy of Sciences, Shanghai 201203, China

^cUniversity of Chinese Academy of Sciences, Beijing 100049, China

^dOral Formulation Development, Novo Nordisk A/S, Maalov 2760, Denmark

^eDepartment of Pharmacy, Faculty of Health and Medical Sciences, University of Copenhagen, Copenhagen 2100, Denmark

^fUniversity of Texas at Dallas, Richardson, TX 75080, USA

^gNMPA Key Laboratory for Quality Research and Evaluation of Pharmaceutical Excipients, National Institutes for Food and Drug Control, Beijing 100050, China

Received 17 May 2021; received in revised form 10 July 2021; accepted 13 July 2021

KEY WORDS

Ligand-modified nanoparticles;
Transporter;
Proton-coupled folate transporter;
Expression level;
Endocytosis;
Intracellular trafficking;
Diabetes;

Abstract Transporters are traditionally considered to transport small molecules rather than large-sized nanoparticles due to their small pores. In this study, we demonstrate that the upregulated intestinal transporter (PCFT), which reaches a maximum of 12.3-fold expression in the intestinal epithelial cells of diabetic rats, mediates the uptake of the folic acid-grafted nanoparticles (FNP). Specifically, the upregulated PCFT could exert its function to mediate the endocytosis of FNP and efficiently stimulate the traverse of FNP across enterocytes by the lysosome-evading pathway, Golgi-targeting pathway and basolateral exocytosis, featuring a high oral insulin bioavailability of 14.4% in the diabetic rats. Conversely, in cells with relatively low PCFT expression, the positive surface charge contributes to the cellular uptake of FNP, and FNP are mainly degraded in the lysosomes. Overall, we emphasize that the upregulated intestinal transporters could direct the uptake of ligand-modified nanoparticles by mediating the endocytosis and

*Corresponding authors. Tel.: +86 021 51322181, fax: +86 021 51322193 (Rui Wang); Tel.: +01 972 883 4480, fax: +01 972 883 4440 (Xiuying Li); Tel.: +86 021 20231975, fax: +86 021 20231000 1425 (Yong Gan).

E-mail addresses: wr@shutcm.edu.cn (Rui Wang), Xiuying.Li@utdallas.edu (Xiuying Li), ygan@simc.ac.cn (Yong Gan).

Peer review under responsibility of Chinese Pharmaceutical Association and Institute of Materia Medica, Chinese Academy of Medical Sciences.

<https://doi.org/10.1016/j.apsb.2021.07.024>

2211-3835 © 2022 Chinese Pharmaceutical Association and Institute of Materia Medica, Chinese Academy of Medical Sciences. Production and hosting by Elsevier B.V. This is an open access article under the CC BY-NC-ND license (<http://creativecommons.org/licenses/by-nc-nd/4.0/>).

Oral insulin delivery

intracellular trafficking of ligand-modified nanoparticles *via* the transporter-mediated pathway. This study may also theoretically provide insightful guidelines for the rational design of transporter-targeted nanoparticles to achieve efficient drug delivery in diverse diseases.

© 2022 Chinese Pharmaceutical Association and Institute of Materia Medica, Chinese Academy of Medical Sciences. Production and hosting by Elsevier B.V. This is an open access article under the CC BY-NC-ND license (<http://creativecommons.org/licenses/by-nc-nd/4.0/>).

1. Introduction

Ligand-modified nanoparticles (LMNPs) binding to specific cell surface targets have potential applications for improving drug delivery efficiency¹. In recent decades, LMNPs specific to receptors have been extensively studied^{2,3}, and the density, length and charge of the ligands have been adjusted to enhance the receptor-targeting abilities, then increasing the cellular internalization of LMNPs^{4,5}. Actually, transporters are also vital membrane transport proteins involved in ion transportation, protein secretion, nutrient capture, and other substance transport⁶. Although transporter-targeted nanoparticles have not been widely explored as it is acknowledged that the pores of transporters are too small for particle transportation⁷, a few reports recently revealed that transporters have been involved in the transportation of LMNPs⁸. For example, the bile acid-conjugated nanocomplexes were reported to be internalized by an apical sodium-dependent bile acid transporter (ASBT)-mediated pathway^{8,9}. Nevertheless, not all the transporters could mediate the endocytosis of LMNPs. It remains unclear how to efficiently boost the transporter-mediated nanoparticle delivery and the detailed transporter-associated transcellular pathways of LMNPs are still blurred.

Intestinal transporters are localized in the cellular membranes of enterocytes and serve as the gatekeepers to govern the uptake of nutrients and drugs¹⁰. Some intestinal diseases might affect the expression and function of intestinal transporters, such as P-glycoprotein^{11,12}, multidrug resistance-associated protein (MRP)^{13,14} and breast cancer resistance protein (BCRP)¹⁵. The affected transporters would further modulate the absorption and distribution of drugs under pathological states^{10,16}. Nevertheless, it is still indistinct whether diabetes would alter the expression levels of intestinal transporters. It was reported that plasma levels of folate and vitamin D were increased in diabetic patients, and the intestinal transportation of folate increased in the diabetic animals^{17,18}. Since folate could mainly be transported by the proton-coupled folate transporter (PCFT) in the intestinal lumen^{19,20}, we hypothesize that PCFT may be upregulated in the diabetes, which could be utilized for enhanced oral drug delivery.

In this study, we revealed that the expressions of PCFT were upregulated in both mRNA and protein levels in the intestinal epithelial cells of diabetic rats, contributing to a unique intestinal pathological characteristic. The upregulated PCFT could exert its function to mediate the endocytosis and intracellular trafficking of the nanoparticles with sufficient folic acid modification (FNP) *via* a PCFT-mediated pathway, leading to a high oral insulin bioavailability of 14.4%. However, in enterocytes with low expression of PCFT, these positively charged FNP were endocytosed by a clathrin-mediated pathway and then were mainly degraded in the lysosomes. This study highlights that the upregulated transporters would

mediate the endocytosis of LMNPs through ligand–transporter interaction and thus change the transcellular itinerary of LMNPs to facilitate oral insulin delivery.

2. Materials and methods

2.1. Materials

Dulbecco's modified Eagle's medium (DMEM), 0.53 mmol/L ethylenediaminetetraacetic acid (EDTA), fetal bovine serum (FBS) and 0.25% trypsin were obtained from Invitrogen (Ontario, Canada). Fluorescein isothiocyanate (FITC), Hoechst 33,258 and RIPA cell lysis buffer were provided by Dalian Meilun Biotech Co., Ltd. (Dalian, China). Chitosan (99% deacetylation and 150 kDa MW) was purchased from Golden-shell Pharmaceutical Co., Ltd. (Hangzhou, China). FITC-labeled porcine insulin (FITC-Ins) was obtained from Jiangsu Wanbang Biochemistry Pharmaceutical Co., Ltd. (Jiangsu, China). 2-(4-Amidinophenyl)-6-indolecarbamidine dihydrochloride (DAPI), secondary antibody anti-mouse IgG (Alexa Fluor 647) and antirabbit IgG secondary antibody (Alexa Fluor 647) were supplied by Beyotime Institute of Biotechnology (Jiangsu, China). Streptozotocin (STZ), paraformaldehyde, poly (g-glutamic acid) (γ -PGA, MW 100 kDa), ethyl urethane, atropine sulfate, 1-(3-dimethylaminopropyl)-3-ethylcarbodiimide hydrochloride (EDC), and myricetin were obtained from Sinopharm Chemical Reagent Co., Ltd. (Shanghai, China). LAMP1 rabbit mAb and Golgi-97 (CDF4) mouse mAb were obtained from Cell Signaling Technology. PCFT (HCP1) rabbit mAb was purchased from Biorbyt (Cambridge, British). Goat anti-rabbit IgG-horseradish peroxidase (HRP), rabbit FL-257 antibody for α -FR, and Texas red-conjugated goat anti-rabbit IgG were all obtained from Santa Cruz Biotechnology (TX, USA). All the reagents were of analytical grade.

2.2. Cell lines and animals

Caco-2 cell lines were obtained from the American Type Culture Collection (ATCC, Manassas, VA, USA). And cells were cultured in DMEM at 37 °C, 5% CO₂. All the media contained 1% penicillin-streptomycin and 10% FBS.

Goto-Kakizaki (GK) rats (male, 10–12 weeks old) and Sprague–Dawley (SD) rats (male, 6–8 weeks old) were provided by the Animal Experimental Center of Shanghai Institute of Materia Medica (IACUC code: 2019-12-GY-55). All the animals had free access to tap water and rat chow. All experimental procedures were executed according to the protocols approved by Institutional Animal Care and under the supervision of Animal Ethics Committee of Shanghai Institute of Materia Medica. STZ-diabetic rats were induced in SD rats (180–200 g, male) *via* an intraperitoneal injection of STZ (65 mg/kg) as previously

described²¹. The blood glucose levels were monitored by a glucose meter (On Call® EZ II, Acon Biotech Co., Ltd., Hangzhou, China). When their fasting blood glucose levels were higher than 16.7 mmol/L after 2-week STZ injection, these rats were considered diabetic.

2.3. RT-qPCR assay

The mRNA levels of *Pcft* and the alpha folate receptor (α -Fr) were assessed in STZ-induced diabetic SD rats, diabetic GK rats and normal SD rats. After fasting for 12 h, rats were sacrificed and the small intestine was obtained and washed with phosphate-buffered saline (PBS, pH = 7.4). The total RNAs were isolated with TRIzol reagent (Invitrogen, Thermo Fisher Scientific, Massachusetts, USA). RNAs were prepared with the RNeasy RNA kit (Qiagen, Valencia, CA, USA). cDNA was produced from 1 μ g of RNAs with the GoScript™ Reverse Transcription System (Promega Corp., Madison, WI, USA). Using the primer sequences listed in Table 1, real-time RT-qPCR was conducted via a 7500 Real-Time PCR System (Applied Biosystems, Foster City, CA, USA). Reduced glyceraldehyde-phosphate dehydrogenase (*Gapdh*) was selected as an internal control for this RT-qPCR analysis. Threshold values (C_t) were used to quantify relative gene expressions using the comparative 2^{- $\Delta\Delta$ CT} method with the ABI 7500 Software Tool (Applied Biosystems).

2.4. Western blot

Sections of different intestinal segments were removed from sacrificed STZ-diabetic SD rats, normal SD rats and GK rats. Enterocytes were isolated following a previously reported procedure²². The proteins were extracted, and the concentrations were tested using the bicinchoninic acid (BCA) assay. The protein extracts were loaded onto a 12% sodium dodecyl sulfate polyacrylamide gel electrophoresis (SDS-PAGE) gel for separation. After proteins were transferred and blocked, rabbit PCFT (HCP1) antibody for PCFT or rabbit FL-257 antibody for α -FR were added at 4 °C overnight and then stained with goat anti-rabbit IgG-HRP at room temperature for 1 h. Tris-buffered saline (TBS) with 0.1% Tween 20 was used to wash all the membranes and then detected by enhanced chemiluminescence (ECL) reaction reagents.

2.5. Immunofluorescence staining

The localization of α -FR and PCFT in the intestinal villi of STZ-diabetic rats was analyzed by immunofluorescence staining. Duodenum, jejunum, and ileum segments were harvested from

sacrificed rats, respectively. Using a cryostat (Leica CM 1950, Germany), cryosections of tissues were cut. The tissue cryosections were blocked with PBS containing 1% bovine serum albumin. Immunofluorescence was performed using rabbit PCFT (HCP1) antibody or rabbit FL-257 antibody and secondary antibody Texas red-conjugated goat anti-rabbit IgG. To investigate the distribution of α -FR and PCFT, the tissue sections were then stained with DAPI and visualized using confocal laser scanning microscopy (CLSM, FV1000, Olympus, Japan).

2.6. Synthesis and characterization of folic acid-grafted chitosan

Briefly, folic acid (FA) and EDC/NHS with a molar ratio of 1:1 were well dissolved in 20 mL anhydrous DMSO. The mixed solution was then slowly added to 0.5% (w/v) chitosan in 1% acetic acid aqueous solution and stirred at room temperature (25 °C) in the dark for 16 h to allow FA grafted onto chitosan molecules. The pH of the mixed solution was brought to pH 9.0 by 2 mol/L NaOH solution and the suspension was then centrifuged at 10,000 \times g for 5 min (Eppendorf, 5424, Hamburg, Germany) to spin down the FA-grafted chitosan. The precipitate was dialyzed first against acetic acid buffer (pH 4.7) for 3 days and then against water for 3 days. Finally, the FA-grafted chitosan was isolated by lyophilization and kept for follow-up study.

Chitosan and FA-grafted chitosan were characterized by ¹H NMR spectroscopy (Avance III 400, Bruker, Switzerland) after dissolving in deuterium acetic acid-d₄ deuterium oxide solution (1%, v/v). Meanwhile, Infrared (IR) spectra were recorded with an IR-200 Thermo-Nicolet 2.2 Spectrometer, in the region of 400–4000 cm⁻¹, with a resolution of 4 cm⁻¹ to confirm the presence of FA groups in FA-grafted chitosan. Freeze-dried FA, chitosan and FA-grafted chitosan were mixed with KBr to prepare pellets.

The FA to amino group molar ratios in FA-grafted chitosan were estimated by the intensity of the absorption maximum (285 nm) of 0.02% FA-grafted chitosan solution with an ultraviolet–visible (UV–Vis) spectrophotometry. FA powder was first dissolved in 0.1 mol/L NaOH solution and diluted to a series of gradient solutions for preparation of the calibration curve in the range from 0.5 to 25.0 μ g/mL.

2.7. Preparation and characterization of nanoparticles with different FA grafting densities

FA-grafted chitosan with different grafting ratios (FA content = 5%, 10%, 20%, *mollmol*) was synthesized following a previously described method with slight changes²³. Insulin was used as the model drug. FITC-Ins loaded FA-grafted chitosan nanoparticles (FNPs, including FNP₅, FNP₁₀ and FNP₂₀) were prepared through self-assembly of the negatively charged FITC-Ins and the positively charged FA-grafted chitosan via electrostatic interaction. γ -PGA was incorporated into nanoparticles to improve the stability at lower pH and high ionic intensity²⁴. Briefly, nanoparticles were prepared by mixing equal volumes of FA-grafted chitosan solution (2 mg/mL), γ -PGA aqueous solution (0.2 mg/mL), and FITC-Ins solution (2 mg/mL) with magnetic stirring at room temperature. To prepare FITC-Ins loaded non-grafted chitosan nanoparticles (NP), chitosan solution (2 mg/mL) instead of FA-grafted chitosan solution was added to the solution at room temperature with magnetic stirring. These nanoparticles were loaded into enteric-coated capsules after freeze-drying following our previously reported method²⁵.

Table 1 Primer sequences of rat *Pcft*, α -Fr and *Gapdh* primers.

Name	Forward/ Reverse	Primer sequence
<i>Pcft</i>	Forward	5'-GCTGCTAGCTTTGCCTCTGT-3'
	Reverse	5'-TGGACTTTGGCTCCTTCACT-3'
α -Fr	Forward	5'-CTGCCATCCCTTCACTTCT-3'
	Reverse	5'-CACTAAGGACAGGCTGCACA-3'
<i>Gapdh</i>	Forward	5'-GGCATTGCTCTCAATGACAA-3'
	Reverse	5'-CCCTGTTGCTGTAGCCGTAT-3'

The mean zeta potential and particle size of nanoparticles were analyzed by Malvern Zetasizer NanoZS (Malvern Instruments, London, UK) and transmission electron microscopy (TEM, Tecnai G2 Spirit, FER, USA) was used to observe the morphology of FNP and NP. Since the nanoparticles were spherical in shape, we calculated the number of chitosan nanoparticles per gram based on the formula for calculating the volume of sphere, in which the density of chitosan was 0.6 g/mL, as previously reported²⁶. After centrifuging nanoparticles at 18,000 rpm for 30 min at 4 °C (Eppendorf HimaC Technologies Co., Ltd., CS120FNX, Ibaraki, Japan), the drug loading efficiency and encapsulation efficiency were calculated by the following equations as described in the literature²⁷ as in Eqs. (1) and (2), after quantifying insulin by high performance liquid chromatography (HPLC).

Encapsulation efficiency

$$= \frac{\text{Total amount of insulin added} - \text{Free insulin}}{\text{Total amount of insulin added}} \quad (1)$$

Loading efficiency

$$= \frac{\text{Total amount of insulin added} - \text{Free insulin}}{\text{Weight of nanoparticles}} \quad (2)$$

2.8. *In vitro* release performances

Nanoparticles were dissolved in 1 mol/L PBS (pH 5, 6.8 and 7.4) and transferred into each dialysis bag (20 kDa molecular weight cut-off, Shanghai Yuanye Bio-Technology Co., Ltd.). These dialysis bags were placed into containers with the respective medium on a shaker at 60 rpm and 37 °C. At predetermined time points (0, 0.5, 1, 1.5, 2, 4, 6, 8, 10, 12 h), samples were removed from the medium for analysis while an equal amount of fresh medium was added. All the samples were centrifuged for 30 min at 16,000×g (Eppendorf HimaC Technologies Co., Ltd., CS120FNX, Ibaraki, Japan), and the final insulin concentration was detected by HPLC.

In addition, circular dichroism (CD) spectra of native insulin and insulin released from nanoparticles were obtained at room temperature on a circular dichroism spectrophotometer (Jasco J-800 Japan) using an insulin concentration of 0.2 mg/mL. In the far-UV region, CD spectra were recorded in a 0.01 cm cell from 250 to 190 nm using a step size of 0.5 nm, a bandwidth of 1.0 nm, and an averaging time of 5 s, with the lamp housing purged with nitrogen to remove oxygen. For all spectra, an average of five scans was obtained. CD spectra of the appropriate reference were recorded and subtracted from the protein spectra.

2.9. *Establishment of high and low expression cell groups*

Caco-2 cells served as the high expression cell group in which PCFT is highly expressed²⁸. To establish the low expression cell group, Caco-2 cells were pretreated with myricetin as an early reported procedure^{28,29}. In short, Caco-2 cells with a seeding density of 1×10^6 cells/well were cultured overnight in 6-well plates and then treated with or without 2 mL myricetin solution (150 μmol/L), distinguished into a low expression group or a high expression group. Then, the cells were rinsed with 1 mL PBS (pH 7.4) and lysed on ice for 20 min using 20 μL RIPA cell lysis

buffer. The extracts were treated as described above, and the expression level of PCFT was detected.

2.10. *Cytotoxicity studies*

The MTT assay was performed to evaluate the cytotoxicity of NP, FNP₅, FNP₁₀ and FNP₂₀ to Caco-2 cells following the standard protocol. The nanoparticle concentrations were 0, 50, 100, 200, 400, 600, 800 and 1000 μg/mL.

2.11. *Cellular uptake studies*

To estimate the uptake of nanoparticles with different grafting densities of FA in Caco-2 cells with high and low expression levels of PCFT, Caco-2 cells were pretreated with Hank's balanced salt solution (HBSS) with or without myricetin (150 μmol/L) for 1 h. NP, FNP₅, FNP₁₀ and FNP₂₀ were used to detect absorption efficiency. After incubation with different nanoparticles (100 μg/mL) for 2 h, the cells were washed, fixed, and stained for CLSM. To quantitatively analyze the fluorescence intensity of FITC-labeled nanoparticles, cells were lysed by RIPA lysis buffer, and then the amounts of nanoparticles and total proteins were determined by an ELISA Kit and BCA Kit, respectively.

To identify the uptake mechanisms of NP, FNP₅, FNP₁₀ and FNP₂₀ in cells with high and low expression of PCFT, cellular uptake experiments were performed with the inhibitors, following a previously reported protocol³⁰. Briefly, myricetin solution (150 μmol/L) was used to pretreat Caco-2 cells (low expression group) for 1 h at 37 °C. In the presence of methyl-β-cyclodextrin, lovastatin, filipin, chlorpromazine and cytochalasin D, cellular uptake mechanism experiments were performed for 1 h at 37 °C. Lovastatin (1 μg/mL) and methyl-β-cyclodextrin (10 mmol/L) were used for cholesterol depletion. Filipin (1 μg/mL) could inhibit the caveolae-mediated endocytosis. Chlorpromazine (10 μg/mL) could inhibit the clathrin-mediated endocytosis. Cytochalasin D (1 μg/mL) could inhibit macropinocytosis.

2.12. *Intracellular transportation studies*

To expound the intracellular transportation of nanoparticles, Caco-2 cells were cultured with FNP₁₀ (hereafter called FNP) and NP for 2 h. PCFT (HCP1) rabbit mAb was used to stain PCFT. LAMP1 rabbit mAb and anti-rabbit IgG Alexa Fluor 647 secondary antibody were used to stain the lysosomes. Golgi-97 (CDF4) mouse mAb and anti-mouse IgG Alexa Fluor 647 secondary antibody were used to stain the Golgi. The colocalization of nanoparticles with PCFT, the lysosomes and the Golgi were imaged using CLSM and analyzed by Fiji ImageJ.

2.13. *Transepithelial transport studies*

The transepithelial transport studies were performed following a previous procedure³¹. Caco-2 cell monolayers with high expression or low expression of PCFT were equilibrated in the $1 \times$ HBSS at 37 °C, and 5% CO₂. FITC-Ins solution (0.5 mg/mL), FNP and NP were diluted to make the concentration of FITC-Ins at 40 μg/mL. After drug administration, 200 μL of sample was removed from the basolateral solution at 0, 15, 30, 45, 60, 90 and 120 min for all the transport experiments. Meanwhile, to maintain a constant volume, 200 μL fresh HBSS was added. All samples were measured using a microplate fluorimeter reader (Model 680,

Bio-Rad, USA) at an excitation filter of 488 nm and an emission filter of 519 nm. The following equation was utilized to calculate the apparent permeability coefficient (P_{app}) as in Eq. (3):

$$P_{app} = \frac{dQ}{dt} \times \frac{1}{A \times C_0} \quad (3)$$

where dQ/dt is the flux of insulin from the apical side to the basolateral side, A is the membrane area (cm^2), and C_0 is the initial concentration of nanoparticles in the apical compartment.

We used 1 mmol/L free FA to presaturate PCFT in Caco-2 cell monolayers for 30 min and then conducted the transport studies.

2.14. Integrity of nanoparticles across the enterocytes

To explore the integrity of nanoparticles transported *via* the PCFT-mediated pathway in Caco-2 cells, the cell monolayers were incubated with the double fluorophore-labeled nanoparticles for 2 h. 200 μL medium was gathered from the apical side and basolateral side. Caco-2 cell monolayers were also collected. The colocalization images of these samples were observed by CLSM.

The FITC-labeled FA-grafted chitosan and FITC-labeled insulin consisted of FNP, which was used as a donor/acceptor pair in the fluorescence resonance energy transfer assay (FRET). The fluorescence intensity was measured using a microplate reader with an excitation wavelength of 450 nm and the fluorescence emission spectrum was measured from 480 to 700 nm.

2.15. *In vivo* absorption studies

To monitor the real-time intestinal transport of insulin, a two-photon microscope was used for intravital imaging as previously reported with minor modifications²⁵. To stain the nuclei of the small intestine epithelial cells, Hoechst 33,258 (1.3 mg/kg) was intraperitoneally injected into the STZ-diabetic SD rats or normal SD rats. Urethane was also injected subcutaneously to anesthetize rats. After the small intestine was exposed, the exposed intestinal lumen was carefully cleared. Time-lapse imaging was immediately conducted using a two-photon microscope (Olympus FV1200MPE, Japan) with a water-immersed 25 \times Objective, after adding different formulations.

The absorption of FNP and NP in intestinal villi was also studied. Before experiments, diabetic and normal SD rats were fasted overnight except for water. Ethyl urethane (20%) was intraperitoneally injected to anesthetize the rats. A 6 cm loop of the jejunum was made by ligation at both ends after the abdomen was exposed. 0.3 mL FNP and NP containing 0.15 mg/mL FITC-Ins were injected into the loop. After incubation, the intestinal loops were harvested, washed, sectioned, and stained for imaging. To study the influence of excessive FA *in vivo*, 1 mmol/L free FA was injected into the diabetic rats for 30 min and the absorption of nanoparticles in intestinal villi was investigated as described above.

2.16. *In vivo* pharmacokinetics-pharmacodynamics studies

Various formulations of nanoparticles, including free insulin solution, enteric capsules containing freeze-dried FNP, free FNP suspension and NP suspension (insulin, 30 IU/kg), were administered *via* gavage to the diabetic rats once a day. Free insulin solution at a dose of 5 IU/kg was subcutaneously injected (SC) as a control group. After dosing, the blood samples were obtained

from the tail veins of rats at various time points (1, 2, 4, 6, 8, 10 and 12 h).

After centrifugation at 3000 rpm for 5 min (Eppendorf, 5424, Hamburg, Germany), blood samples were subsequently quantified using insulin enzyme-linked immunosorbent assay (ELISA) kits (Merckodia AB, Sweden) to analyze the serum insulin levels. The relative bioavailability (F%) and pharmacological bioavailability (PA%) of FNP and NP were calculated using the following Eqs. (4) and (5):

$$F(\%) = \frac{\text{AUC(oral)} \times \text{Dose(sc)}}{\text{AUC(sc)} \times \text{Dose(oral)}} \times 100 \quad (4)$$

$$\text{PA}(\%) = \frac{\text{AAC(oral)} \times \text{Dose(sc)}}{\text{AAC(sc)} \times \text{Dose(oral)}} \times 100 \quad (5)$$

2.17. Statistical analysis

All the data were shown as the means \pm standard error of the mean (SEM). We used several software for data processing, such as R, MATLAB and Python. Student's *t*-test (SPSS, Chicago, IL) were utilized to compare the two groups while one-way analysis of variance (ANOVA) with Tukey's *post-hoc* test was applied to compare multiple groups. n.s. $P > 0.05$, * $P < 0.05$, ** $P < 0.01$, *** $P < 0.001$.

3. Results and discussion

3.1. The upregulation of PCFT in the diabetic rats

The intestinal folate transport systems (PCFT, α -FR and the reduced folate carrier) are reported to participate in the transportation and tissue distribution of folate³². In view of that the reduced folate carrier only transports reduced folate at neutral pH³³, we focused on PCFT and α -FR for the following studies. Here, we conducted an RT-qPCR assay to analyze the mRNA expression levels of two intestinal folate transport proteins in STZ-induced diabetic SD rats, diabetic GK rats and normal SD rats. The results showed that the expressions of α -FR and PCFT reached a maximum of 19.8- and 12.3-fold increase in the STZ-diabetic rats compared to that in the normal rats, respectively (Fig. 1A and Supporting Information Fig. S1A). In addition, we used diabetic GK rats to check whether this phenomenon could be observed in other diabetes mellitus. The results demonstrate that the mRNA expression levels of the two folate transport systems were also significantly increased in the GK rats. We next investigated the expressions of the three folate transport systems in the protein levels by using a Western blot. As we expected, Western blot results also verified that the protein expression levels of α -FR and PCFT were both upregulated in diabetes mellitus (Fig. 1B and Fig. S1B). The upregulation of PCFT was higher in the proximal intestine of the diabetic rats, while the expression of α -FR significantly increased in the distal intestinal tract of the diabetic rats (Fig. 1C and Fig. S1C). Furthermore, immunofluorescent staining of α -FR and PCFT in fixed intestinal tissues was performed to reveal their distribution patterns. In accordance with previous results³⁴, our results showed that α -FR was mainly expressed in the nuclei of the intestinal epithelial cells (Fig. S1D), which completely differed from the cellular surface distribution of α -FR in tumor cells^{35,36}. Since the ligand-receptor interaction on the cellular surface is a prerequisite for receptor-mediated

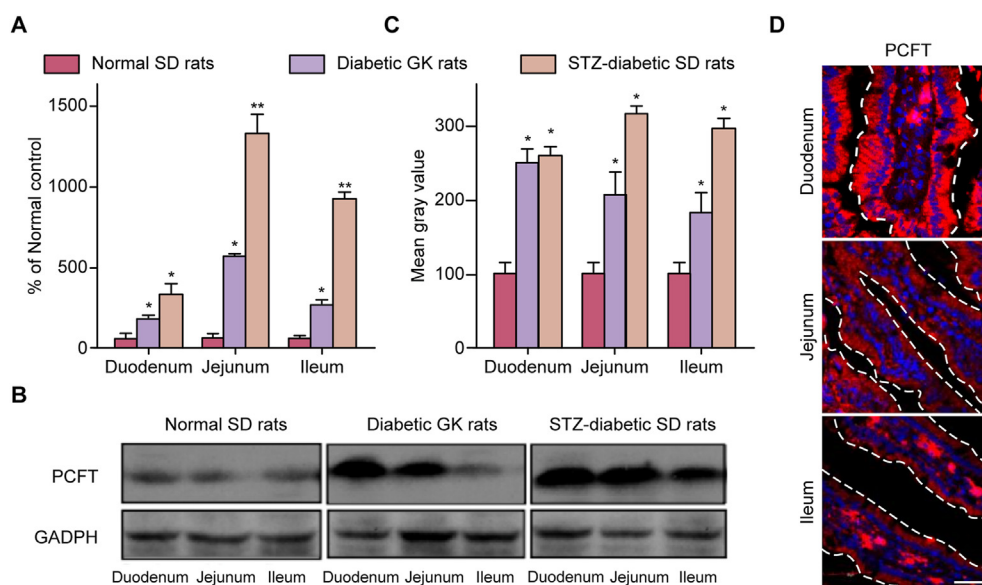


Figure 1 The expression levels of PCFT in the diabetes. (A) mRNA levels of PCFT in normal SD rats, STZ-diabetic SD rats and diabetic GK rats. Data are mean \pm SD ($n = 6$); * $P < 0.05$, ** $P < 0.01$. PCFT was upregulated in the diabetic rats. (B) Western blot images of PCFT in the three species of rats (C) Protein levels of PCFT in the three species of rats. Data are mean \pm SD ($n = 6$); * $P < 0.05$, ** $P < 0.01$. (D) Immunofluorescent images of PCFT (red) in the intestinal villi sections (blue) of the STZ-diabetic rats. Scale bar = 50 μm .

endocytosis, α -FR may not mediate the internalization of LMNPs directly. By contrast, PCFT was localized in the apical membrane and cytosol of intestinal epithelium cells throughout the intestine, and thus might play the primary role in the transport process of folate derivatives (Fig. 1D). Therefore, we focused on the interaction between PCFT and FA-grafted nanoparticles for further transcellular delivery studies *in vitro* and *in vivo*.

3.2. Preparation and characterization of FA-grafted nanoparticles

To study the different delivery efficiencies of nanoparticles under pathological conditions and normal conditions, FA-grafted nanoparticles that could target to PCFT were prepared and non-grafted nanoparticles were also prepared as control groups^{37,38}. FA was covalently conjugated to chitosan *via* its γ -carboxyl moiety by an EDC/NHS-mediated reaction (Fig. 2A). The synthesis of FA-chitosan conjugates was confirmed by ¹H-NMR spectroscopy. The signals appearing at δ 6.3–8.5 ppm in the ¹H-NMR spectra were attributed to the resonance of FA aromatic protons, revealing that FA was successfully conjugated to the chitosan backbone (Fig. 2B). The FTIR spectra of free FA, chitosan and FA-grafted chitosan were shown in Fig. S2. Chitosan showed the characteristic IR bands at 1078 cm^{-1} (C–O stretch), 1149 cm^{-1} (bridge–O stretch), 1589 cm^{-1} (NH bend), and 2–877 cm^{-1} (C–H stretch). FA-grafted chitosan exhibited not only the characteristic bands of the original chitosan but also the characteristic peaks of FA at 1490 cm^{-1} (–NH amide band II) and 1603 cm^{-1} (–CONH amide band II), in agreement with a previous report^{39,40}. In addition, the molar ratios of FA to amino group could be modulated from 0.001 to 0.005 by different initial FA to chitosan ratios (Supporting Information Fig. S3).

Oral insulin is the Holy Grail of the diabetes treatment. Herein, insulin was adopted as the model drug loaded into nanoparticles. The nanoparticles were spontaneously formed by adding γ -PGA and FITC-Ins into FA-grafted chitosan with different FA ratios,

respectively (Fig. 2C). The morphology of NP, FNP₅, FNP₁₀ and FNP₂₀ was observed by TEM, and the nanoparticles were spherical in shape and approximately 200 nm in size (Fig. 2D). The hydrodynamic diameters and zeta potentials of NP, FNP₅, FNP₁₀ and FNP₂₀ were also measured (Fig. 2E). FNPs were equipped with excellent encapsulation efficiency and loading efficiency due to their high protein association capacity (Table 2). The release profiles at different pH values (pH 5.0, 6.8 and 7.4) in simulated intestinal medium showed that less than 30% of insulin was released from nanoparticles under weakly acidic environments, and there was no significant difference among different nanoparticles (Fig. 2F and Supporting Information Fig. S4A–S4C). The CD spectra of native insulin and insulin released from FNPs and NP were displayed in Fig. S4D. The native insulin showed two minima at 210 and 223 nm. And no substantial alteration was observed in insulin released from FNPs and NP, suggesting that the secondary structure of insulin encapsulated in FNPs and NP remained unchanged.

3.3. Cellular uptake studies of FA-grafted nanoparticles

Caco-2 cells are human epithelial colorectal adenocarcinoma cells with high expression of PCFT^{28,32}, which usually served as a well-established *in vitro* cell model for intestinal absorption. To explore the influence of PCFT expression levels on nanoparticle uptake, myricetin was applied to inhibit the PCFT expression^{28,29,41}. Caco-2 cells without myricetin pretreatment were regarded as the high expression group, and Caco-2 cells with myricetin pretreatment were regarded as the low expression group (Fig. 3A). The MTT results show that the nanoparticles were nontoxic at the tested concentrations (Supporting Information Fig. S5). Cellular uptake of the nanoparticles in Caco-2 cells was visualized using CLSM. In the high expression group, the cellular uptake of FNP₁₀ and FNP₂₀ was significantly greater than that of FNP₅ and NP (Fig. 3B, top and Fig. 3C). However, owing to their positively charged surfaces, the nanoparticles possessed potent electrostatic

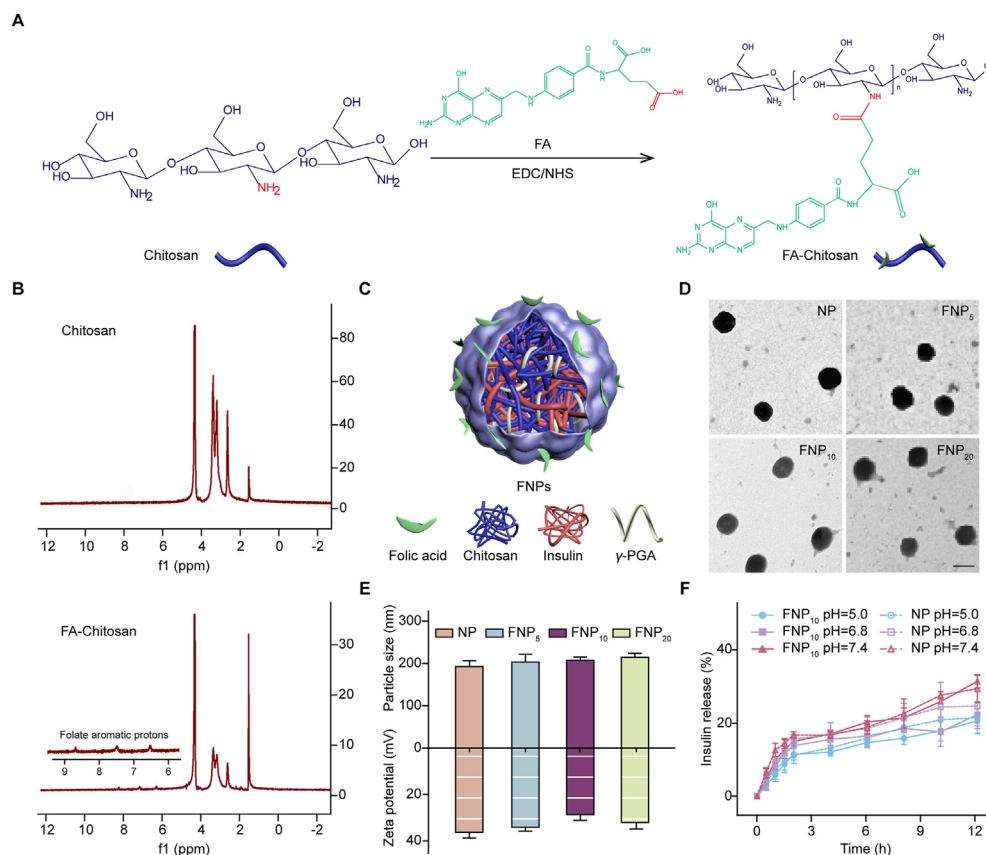


Figure 2 Synthesis and characterization of FA-grafted nanoparticles and non-grafted nanoparticles. (A) Schematic illustration of the synthesis of FA-grafted chitosan. FA was covalently conjugated to chitosan by an EDC/NHS-mediated reaction (B) ^1H NMR spectra of chitosan (top) and FA-grafted chitosan (bottom). (C) Schematic representation of FNPs structure. FNPs were fabricated by the self-assembly of FA-grafted chitosan with different FA ratios, FITC-Ins and γ -PGA (D) TEM images of NP, FNP₅, FNP₁₀ and FNP₂₀. Scale bar = 200 nm. (E) Hydrodynamic diameters and zeta potentials of NP, FNP₅, FNP₁₀ and FNP₂₀ (F) Insulin release profiles from FNP₁₀ (solid lines) and NP (dashed lines) at pH 5.0, pH 6.8 and pH 7.4, respectively. Data are mean \pm SD ($n = 3$).

interaction with the negatively charged cellular membranes in the low expression group. As a result, the cellular uptake of NP was equivalent to that of FNP₅, FNP₁₀ and FNP₂₀ (Fig. 3B, bottom and Fig. 3C).

We next utilized different endocytosis inhibitors to explore the endocytosis mechanisms of the nanoparticles. Methyl- β -cyclodextrin and lovastatin were used for cholesterol depletion, inhibiting the caveolae- and clathrin-independent endocytosis. The caveolae-mediated endocytosis was inhibited by filipin.

Chlorpromazine would inhibit clathrin-mediated endocytosis and cytochalasin D could inhibit macropinocytosis. As shown in Fig. 3D–F, the cellular uptake of FNPs and NP markedly decreased at 4 °C in both high and low expression groups, which suggested that the internalization of FNPs and NP was energy-dependent. In the low expression group, the absorption of all the nanoparticles was reduced by chlorpromazine which proved that they were internalized by clathrin-mediated endocytosis (Fig. 3F, bottom). Conversely, in the high expression group, these results

Table 2 Particle size, polydispersity index, zeta potential, encapsulation and loading efficiency of nanoparticles.

Nanoparticle parameter	NP	FNP ₅	FNP ₁₀	FNP ₂₀
Particle size (nm)	193.9 \pm 13.6	207.6 \pm 15.4	216.7 \pm 16.8	224.3 \pm 11.9
Polydispersity index	0.202 \pm 0.015	0.113 \pm 0.021	0.245 \pm 0.018	0.193 \pm 0.024
Zeta potential (mV)	35.5 \pm 2.3	33.7 \pm 1.1	28.5 \pm 1.8	30.2 \pm 1.3
FA content (% mol)	—	5.0	10.0	20.0
FA to amino group ratio (%)	—	1.12 \pm 0.03	2.28 \pm 0.03	4.45 \pm 0.05
Estimated FA density (per nanoparticle) ^a	—	242	331	565
Encapsulation efficiency	73.5 \pm 4.1%	78.4 \pm 6.1%	83.3 \pm 2.4%	84.1 \pm 3.0%
Loading efficiency	42.4 \pm 1.4%	42.7 \pm 1.9%	45.4 \pm 0.7%	47.1 \pm 1.3%

—, not applicable.

^aFA density was calculated by normalizing the FA content with the number of nanoparticles, assuming that the nanoparticles were spherical in shape. Data are mean \pm standard error.

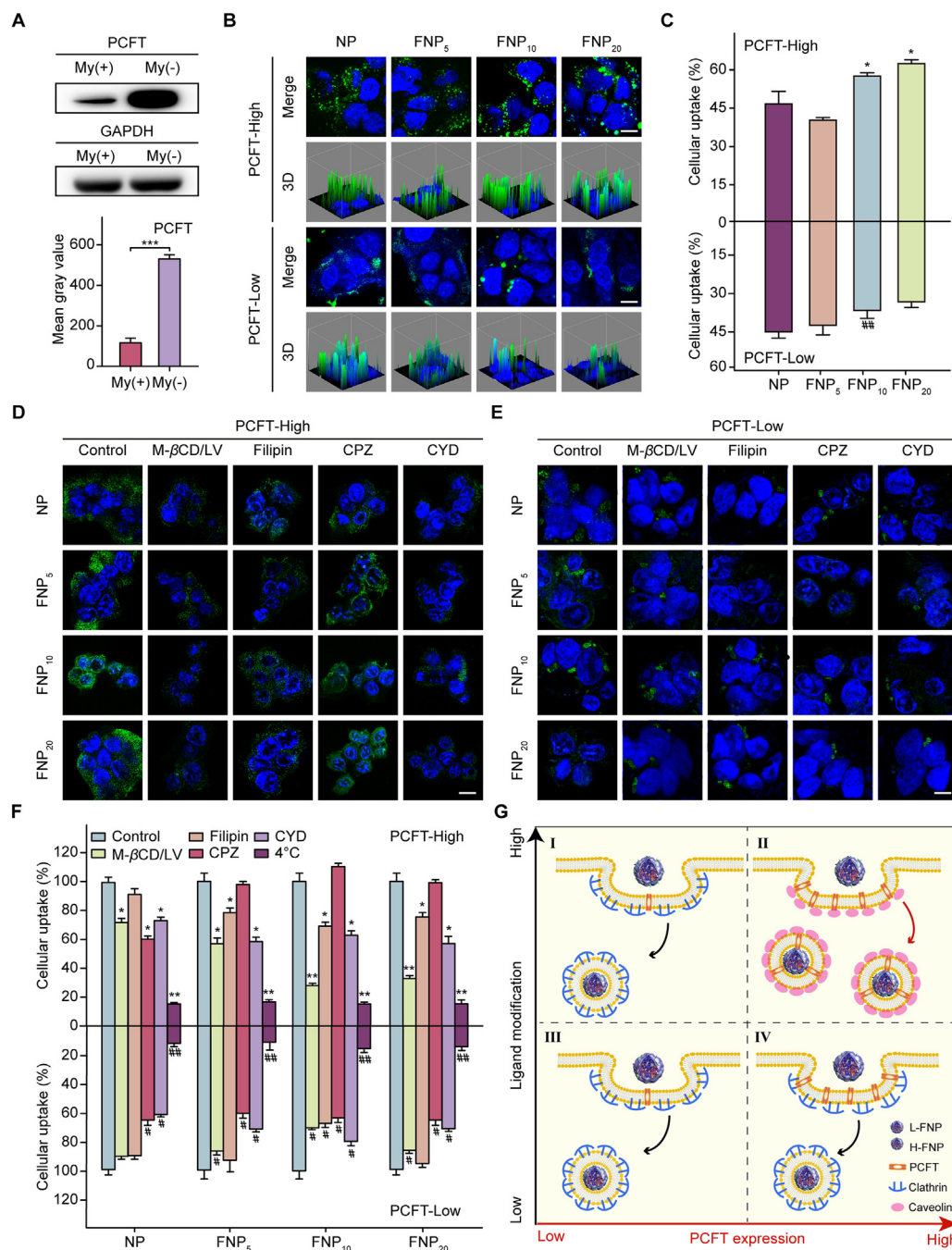


Figure 3 Cellular uptake studies of the nanoparticles (NP, FNP₅, FNP₁₀ or FNP₂₀) in Caco-2 cells with different PCFT expression levels. (A) Western blot and the mean gray value of PCFT in Caco-2 cells ($n = 6$). My (+), with myricetin pretreatment, My (-), without myricetin pretreatment. (B) CLSM images (top) and 3D surface plots (bottom) of nanoparticles (green) in Caco-2 cells (blue). PCFT-High, without myricetin pretreatment, PCFT-Low, with myricetin pretreatment. (C) Cellular uptake of the nanoparticles. Data are mean \pm SD ($n = 3$); * $P < 0.05$, ** $P < 0.01$, compared with the cellular uptake of FNP₅ in PCFT-High, ## $P < 0.01$, compared with the cellular uptake of FNP₁₀ in PCFT-High. (D)–(E) CLSM images of the endocytosis mechanisms of nanoparticles (green) in Caco-2 cells (blue) pretreated with different inhibitors. CPZ, chlorpromazine; LV, lovastatin; M-βCD, methyl-β-cyclodextrin; CYD, cytochalasin D. (F) Quantification of nanoparticles internalized in Caco-2 cells. Data are mean \pm SD ($n = 3$); * $P < 0.05$, ** $P < 0.01$, compared with the Control per group in PCFT-High, # $P < 0.05$, compared with the Control per group in PCFT-Low. (G) Schematic illustrations of the nanoparticle endocytosis pathways. L-FNP, nanoparticles modified with a low density of FA, H-FNP, nanoparticles modified with a high density of FA. When the FA modification was low, the FA-grafted nanoparticles were internalized by the clathrin-mediated pathway (III, IV). Despite the high FA modification, high PCFT expression was required to stimulate efficient ligand–transporter interaction, which led to the internalization of FA-grafted nanoparticles by the caveolae-mediated pathway (II) rather than by the clathrin-mediated pathway in low expression of PCFT (I). Scale bar = 10 μm.

clarified that NP were internalized by the clathrin-mediated pathway and macropinocytosis (Fig. 3F, upper), which was in agreement with a previous report⁴². For FNP₁₀ and FNP₂₀, the uptake of the nanoparticles was reduced by about 70% when cholesterol was depleted, and about 30% after the addition of filipin. The internalization of FNP₁₀ and FNP₂₀ was mainly related to caveolae-mediated endocytosis and caveolae- and clathrin-independent endocytosis, probably associated with upregulated folate transporters. However, FNP₅ were internalized by a similar pathway to NP, which proved that the sufficient FA grafting density was essential to change the cellular uptake pathway of FA-modified nanoparticles.

As concluded in Fig. 3G, two preliminaries that were sufficient FA modification [FA content (% *mollmol*) of 10.0 here, corresponding to 331 ligands per nanoparticle] and high PCFT expression (at least 5.2-fold increase as Fig. 3A) were required to stimulate efficient ligand–transporter interaction, which altered the internalization of LMNPs to caveolae-mediated endocytosis. Otherwise, most nanoparticles were endocytosed by the clathrin-mediated pathway. In the following studies, we chose FNP₁₀ (FA content (% *mollmol*) as 10.0, hereafter called FNP) for further studies.

3.4. The traverse of FNP across the enterocytes

Normally, nanoparticles inevitably face the lysosomal degradation after the receptor-mediated endocytosis (also known as clathrin-dependent endocytosis)⁴³. Transporters are not regarded to transport nanoparticles in most cases due to their small pores⁷. However, there are some transporters, such as ASBT, sodium dependent multivitamin transporters and plasma membrane monoamine transporters, that mediate the cellular uptake of nanoparticles^{8,44}.

In this study, to investigate whether the upregulated PCFT could mediate the endocytosis of FNP and further change the transcellular pathway of FNP directly, we conducted intracellular trafficking experiments (Fig. 4A–F). The colocalization ratios were evaluated by the Pearson's correlation coefficient. In the high expression group, the colocalization ratios of FNP with PCFT and the Golgi were approximately 0.72 and 0.54 respectively, indicating that FNP were mainly colocalized with PCFT and the Golgi. Whereas, NP were colocalized with the lysosomes, indicating that NP were trapped in the lysosomes and degraded later. In the low expression group, both FNP and NP mainly colocalized with the lysosomes. Based on the above data, we came to a conclusion that FNP could interact with the upregulated PCFT, then be endocytosed through the PCFT-mediated pathway, and be further transported *via* the Golgi pathway.

3.5. Transepithelial transport studies of FNP

The transcellular permeability of FNP or NP was analyzed in Caco-2 cell monolayers. In the high expression group, the P_{app} of FNP across Caco-2 monolayers was 4.15×10^{-6} cm/s (Fig. 4G), which was 2.2- and 18.1-fold compared to NP and free insulin, respectively. The P_{app} of FNP across Caco-2 monolayers in the low expression group was half of that in the high expression group. In addition, after blocking the PCFT with free FA, the P_{app} of FNP was dramatically reduced, similar to NP (Supporting Information Fig. S6). Overall, the permeability of insulin loaded in the FNP was significantly improved in the high expression group.

Although chitosan is widely utilized for oral delivery^{45,46}, reports indicate that chitosan might reversibly open tight junctions⁴⁷. The transepithelial electrical resistance (TEER) values of Caco-2 cell monolayers before and after the treatment of FNP or NP were then monitored to confirm the integrity of the tight junctions⁴⁸. There was no significant reduction when Caco-2 cell monolayers were treated with FNP and NP (Supporting Information Fig. S7). The results suggest that the permeability of the nanoparticles across Caco-2 cell monolayers was enhanced by the transcellular transport rather than the paracellular transport. In addition, CLSM and FRET were conducted to confirm the integrity of nanoparticles in the transcellular process after incubation in Caco-2 cell monolayers (Fig. 4H and Supporting Information Figs. S8–S11). The emission of FNP and NP was increased at 580 nm, stating that nanoparticles could remain intact during the transcellular process.

To sum up, owing to this upregulation, FNP were transported *via* the PCFT-mediated pathway. Specifically, the upregulated PCFT could mediate the endocytosis of FNP by a caveolae-mediated pathway and FNP were further transported through the Golgi pathway for efficient exocytosis, thus enhancing the transcytosis of insulin. In contrast, these positively charged FNP were endocytosed by a clathrin-mediated pathway in the PCFT low expression group, and then mainly degraded in the lysosomes (Fig. 4I).

3.6. In vivo intestinal absorption of insulin

Since the improved nanoparticle absorption was confirmed *in vitro*, we further investigated the real-time uptake of insulin from the nanoparticles in the small intestine villi using two-photon microscopy⁴⁹. The results showed that little insulin from FNP was absorbed in the normal rats (Fig. 5A, Supporting Information Video S3), almost equal to the intestinal uptake of insulin from NP in the diabetic rats and normal rats (Supporting Information Videos S4 and S5). However, a great deal of insulin from FNP was absorbed in the diabetic rats (Supporting Information Video S1). Insulin from FNP was observed not only in gaps between each villus (indicated as white arrows) but also inside the villus (indicated as red arrows). In addition, the intestinal uptake of insulin was dramatically decreased when PCFT was presaturated with excess amount of freeFA (Supporting Information Fig. S12 and Video S2), indicating that the upregulated PCFT contributed to the enhancement of insulin absorption after loading into FNP. CLSM imaging and quantification analysis of the intestinal villi were in agreement with the two-photon microscope imaging results (Fig. 5B and C). In addition, most FNP were colocalized with PCFT in the diabetic rats, as the colocalization ratio of FNP with PCFT was 0.81 (Fig. 5D and Supporting Information Fig. S13). These results demonstrate that the absorption of insulin could be notably improved as a result of the accelerated FNP uptake mediated by the upregulated PCFT.

3.7. In vivo pharmacological and pharmacokinetic studies

We finally evaluated the hypoglycemic response of four insulin formulations (insulin solution, enteric capsules containing FNP, FNP suspension and NP suspension) in fasted diabetic rats (Fig. 5E). Freeze-dried FNP were loaded into enteric-coated capsules, which would release nanoparticles in the intestine. The orally administered insulin solution did not generate a significant glucose response in the diabetic rats, whereas subcutaneous

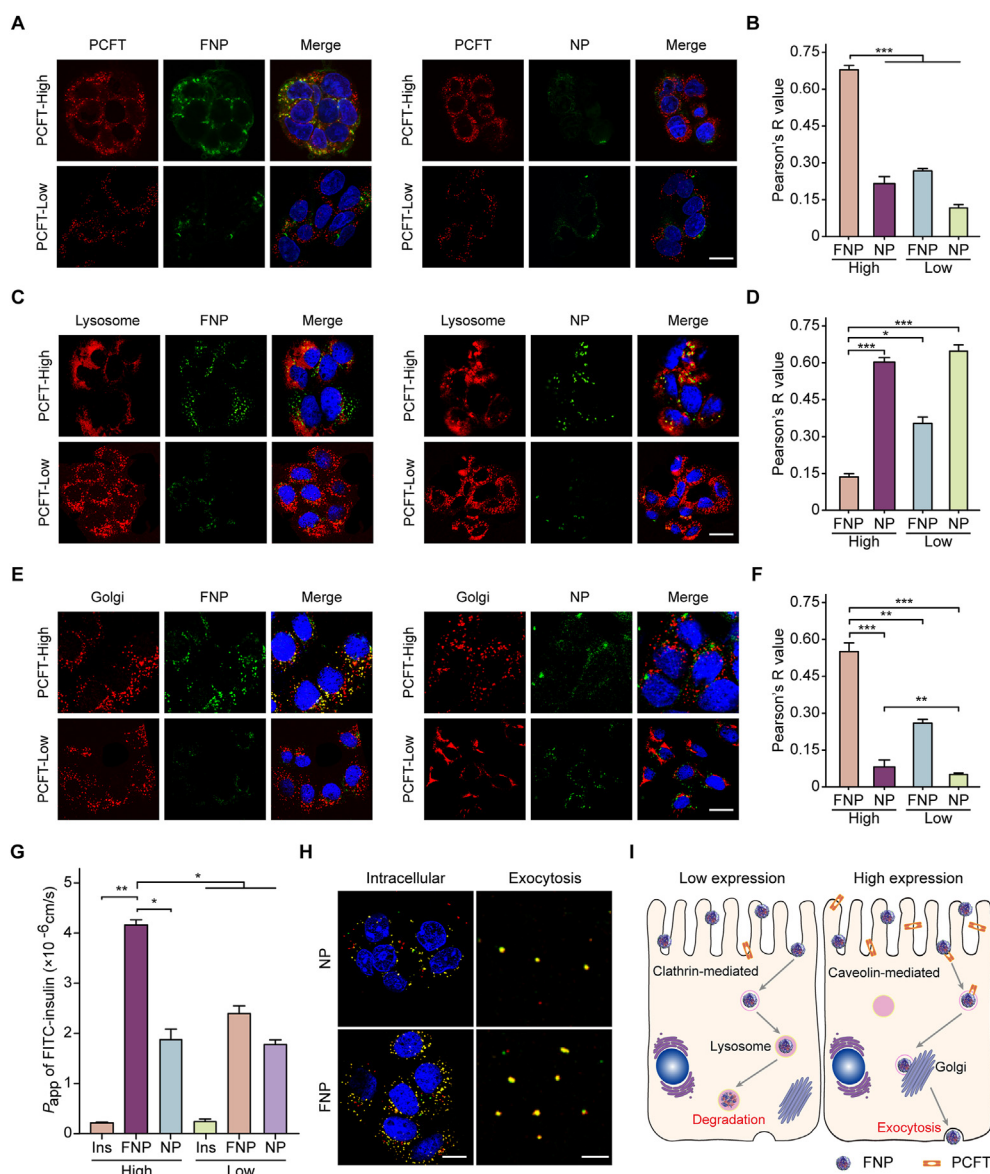


Figure 4 Intracellular pathways of FNP and NP in the PCFT high expression group and PCFT low expression group. (A) CLSM colocalization images of FNP (green, left) or NP (green, right) with PCFT (red) in the PCFT high expression group (PCFT-High, top) and PCFT low expression group (PCFT-Low, bottom). (B) Pearson's correlation coefficient of nanoparticles and PCFT. FNP colocalized with PCFT when PCFT highly expressed (C) CLSM colocalization images of nanoparticles (green) in the lysosomes (red). (D) Pearson's correlation coefficient of nanoparticles and the lysosomes (E) CLSM colocalization images of nanoparticles (green) in the Golgi (red). (F) Pearson's correlation coefficient of nanoparticles and the Golgi. FNP were transported to the Golgi in the PCFT high expression group (G) P_{app} of FITC-Ins, FNP and NP in the two groups. (H) CLSM colocalization images of the nanoparticles internalized by the PCFT-mediated pathway and after exocytosis (I) Schematic of the transcellular pathways of FNP in PCFT-Low (left) and PCFT-High (right). Scale bar = 10 μ m. Data are mean \pm SD ($n = 3$); * $P < 0.05$, ** $P < 0.01$, *** $P < 0.001$.

injection of insulin solution created a rapid glucose response. Capsules containing FNP induced a significant hypoglycemic response, reducing the glucose level within 2 h after administration. The blood glucose level decreased to 40% of the baseline after 8 h, and the hypoglycemic effect lasted more than 10 h after oral administration. The pharmacological bioavailability (PA%) of capsules containing FNP was about 17.4% based on area above the curve (AAC) with the profile of Fig. 5E. FNP suspensions also triggered a slight hypoglycemic effect, which was better than that of the NP suspension.

The serum insulin concentration was measured by ELISA kits. The pharmacokinetic parameters of different formulations were listed in Table 3, and most orally administered formulations reached the maximum serum insulin concentration within 4 h. Fig. 5F shows a rapid increase in serum insulin concentration in the diabetic rats subcutaneously treated with free insulin solution. Oral administration of enteric capsules with FNP presented the highest serum insulin level among the diabetic rats treated with other formulations, showing an oral insulin bioavailability of 14.4%. We also tested the serum insulin concentration of enteric

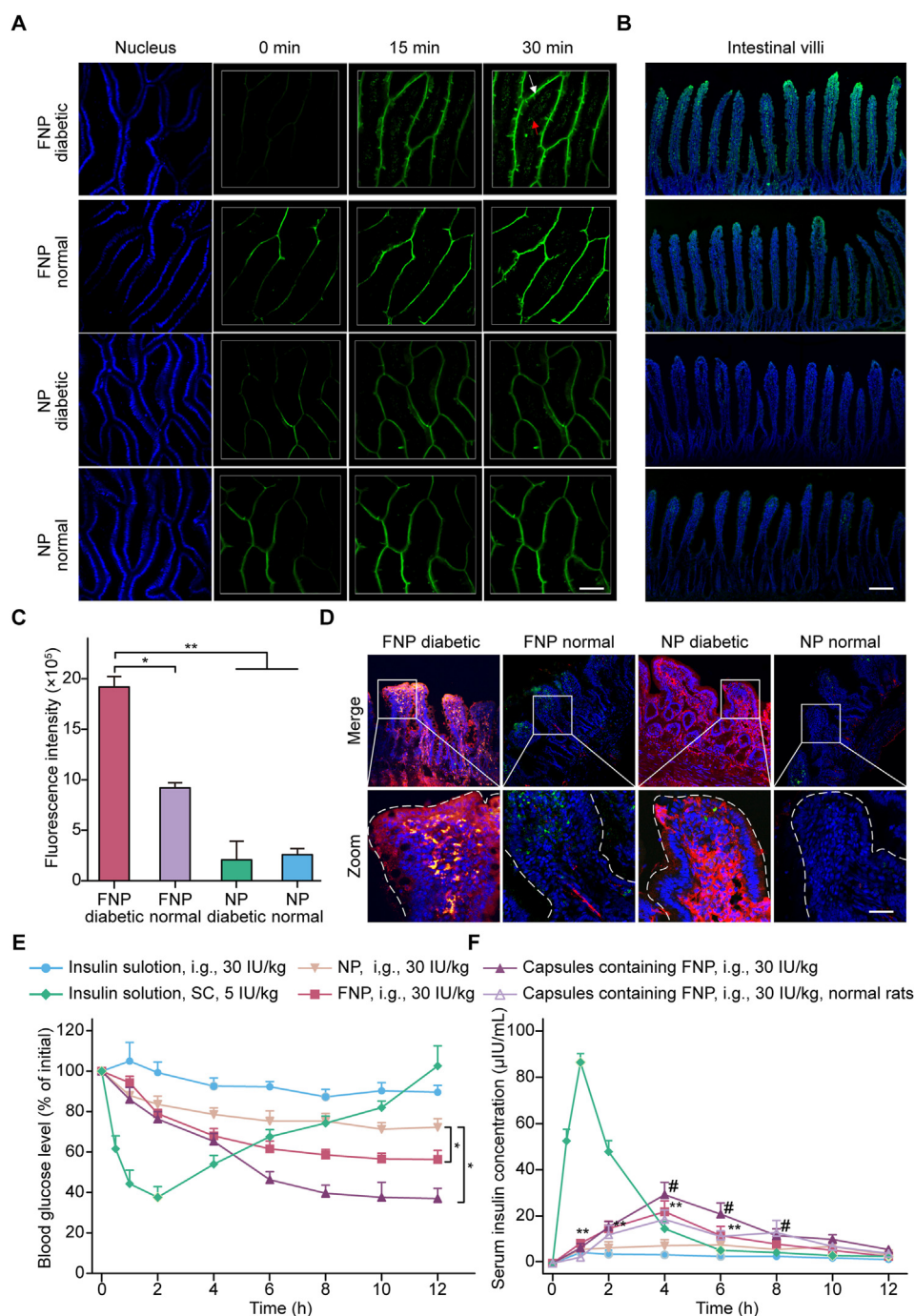


Figure 5 *In vivo* intestinal absorption of insulin from nanoparticles. (A) Two-photon microscopy images of the absorption process of FNP (green) or NP (green) in the small intestine of the diabetic rats and the normal rats ($n = 6$). The pictures were captured at 0, 15 and 30 min, respectively. Scale bar = 30 μm . (B) CLSM images of the small intestinal villi after nanoparticle incubation. Scale bar = 300 μm . (C) Fluorescence intensity of the nanoparticles in two-photon images at 30 min. Data are mean \pm SD ($n = 6$); * $P < 0.05$, ** $P < 0.01$. (D) CLSM colocalization images of FNP (green) or NP (green) with PCFT (red) in the diabetic rats and the normal rats. Scale bar = 50 μm . (E) Blood glucose level of STZ-diabetic rats ($n = 6$) following oral administration of FNP, NP, enteric capsules containing FNP, and insulin solution, as well as subcutaneous injection of insulin solution. (F) Serum insulin levels vs. time profiles of diabetic rats ($n = 6$) and normal rats ($n = 6$) following the administration of the same formulations in (E). Data are mean \pm SD, * $P < 0.05$, compared to NP, ** $P < 0.01$, compared to NP, # $P < 0.05$, compared to enteric capsules containing FNP tested in the normal rats.

capsules with FNP in normal rats. It was worth noting that the absorption enhancement was significantly minimized and the relative bioavailability was decreased from 14.4% to 9.2%.

Besides, the serum insulin level in the diabetic rats treated with FNP suspension was increased, with an $\text{AUC}_{0-12\text{h}}$ of $122.1 \pm 22.4 \mu\text{IU}\cdot\text{h/mL}$ and a relative bioavailability of 9.5%. In summary,

Table 3 Pharmacokinetic and pharmacological parameters of FNP, NP and free insulin (S) after administration to the diabetic or normal rats.

Parameter	S (SC)-D	FNP (i.g.)-D	NP (i.g.)-D	S (i.g.)-D	FNP-C (i.g.)-D	FNP-C (i.g.)-N
Dose (IU/kg)	5.0	30.0	30.0	30.0	30.0	30.0
AUC ($\mu\text{IU}\cdot\text{h/mL}$)	214.0 \pm 33.1	122.1 \pm 22.4	67.2 \pm 6.8	11.5 \pm 0.5	184.9 \pm 49.7	118.7 \pm 20.1
C_{max} ($\mu\text{IU/mL}$)	87.7	21.5	9.8	1.2	32.3	17.7
T_{max} (h)	1.0	4.0	4.0	1.0	4.0	4.0
F	100%	9.5%	5.2%	0.8%	14.4%	9.2%

Note: S, free insulin solution; FNP-C, FNP capsule; D, the diabetic rats; N, the normal rats. Data are mean \pm standard error.

FNP eventually enhanced the oral insulin delivery with efficient hypoglycemic function attributed to the upregulated PCFT in the diabetic rats.

4. Conclusions

Herein, we discovered that the intestinal transporters upregulated in the diabetes could mediate the endocytosis of LMNPs, subsequently changed the intracellular transport of LMNPs, and eventually improved the absorption of the loaded insulin *in vivo*. Specifically, we demonstrated that FNP grafted with a proper density of FA were internalized *via* the PCFT-mediated pathway in enterocytes with high expression of PCFT, and then were transported through the Golgi pathway for efficient exocytosis. Conversely, these positively charged FNP were endocytosed by the clathrin-mediated pathway and were transferred through the lysosome pathway while PCFT was previously inhibited or expressed at low levels. In the diabetic rats, FNP could interact with the upregulated PCFT and then were largely transported across enterocytes in the small intestine, contributing to a high oral insulin bioavailability of 14.4%. Remarkably, this study reveals that the upregulation of intestinal transporters under disease states is essential to stimulate ligand–transporter interaction and the transporter-mediated uptake of nanoparticles. LMNPs could be transported across enterocytes *via* this distinct transporter-mediated pathway, evading the lysosomal degradation for efficient exocytosis. We believe that this discovery would theoretically offer an innovative perspective for rational design of transporter-targeted nanoparticles for enhanced oral drug delivery in diverse diseases.

Acknowledgments

The authors thank the financial support from the National Natural Science Foundation of China (NSFC, No. 81773651, 82025032, and 81803445, China), NN-CAS foundation, National Key R&D Program of China (No. 2020YFE0201700, China), and Major International Joint Research Project of Chinese Academy of Sciences (No. 153631KYSB20190020, China). We would like to thank Dr. Ulrik Lytt Rahbek from Novo Nordisk A/S, Denmark, for helpful discussion about folate receptors and transporters. We also thank the National Center for Protein Science Shanghai for two-photon intravital imaging of experimental rats.

Author contributions

Yong Gan, Xiuying Li and Rui Wang conceived the concept. Jingyi Li, Yaqi Zhang and Miaorong Yu designed the experiments. Jingyi Li and Yaqi Zhang et al. did most of experiments. All of the authors joined in pertinent experiments and manuscript writing.

Conflicts of interest

The authors declare that they have no known competing financial interests or personal relationships that could have appeared to influence the work reported in this paper.

Appendix A. Supporting information

Supporting data to this article can be found online at <https://doi.org/10.1016/j.apsb.2021.07.024>.

References

- Lundquist P, Artursson P. Oral absorption of peptides and nanoparticles across the human intestine: opportunities, limitations and studies in human tissues. *Adv Drug Deliv Rev* 2016; **106**:256–76.
- Safari H, Kelley WJ, Saito E, Kaczorowski N, Carethers L, Shea LD, et al. Neutrophils preferentially phagocytose elongated particles—an opportunity for selective targeting in acute inflammatory diseases. *Sci Adv* 2020;6. eaba1474.
- Bellini M, Riva B, Tinelli V, Rizzuto MA, Salvioni L, Colombo M, et al. Engineered ferritin nanoparticles for the bioluminescence tracking of nanodrug delivery in cancer. *Small* 2020; **16**:e2001450.
- Wang SH, Dormidontova EE. Nanoparticle design optimization for enhanced targeting: Monte Carlo simulations. *Biomacromolecules* 2010; **11**:1785–95.
- Qu Y, Wu ZT, Liu Y, Lin JH, Zhang L, Luo XL. Impact of double-chain surfactant stabilizer on the free active surface sites of gold nanoparticles. *Mol Catal* 2021; **501**:111377.
- Webster P, Saito K, Cortez J, Ramirez C, Baum MM. Concentrative nucleoside transporter 3 is located on microvilli of vaginal epithelial cells. *ACS Omega* 2020; **5**:20882–9.
- Hu NJ, Iwata S, Cameron AD, Drew D. Crystal structure of a bacterial homologue of the bile acid sodium symporter ASBT. *Nature* 2011; **478**:408–11.
- Park J, Choi JU, Kim K, Byun Y. Bile acid transporter mediated endocytosis of oral bile acid conjugated nanocomplex. *Biomaterials* 2017; **147**:145–54.
- Fan WW, Xia DN, Zhu QL, Li XY, He SF, Zhu CL, et al. Functional nanoparticles exploit the bile acid pathway to overcome multiple barriers of the intestinal epithelium for oral insulin delivery. *Biomaterials* 2018; **151**:13–23.
- Drozdziak M, Czekawy I, Oswald S, Drozdziak A. Intestinal drug transporters in pathological states: an overview. *Pharmacol Rep* 2020; **72**:1173–97.
- Erdmann P, Bruckmueller H, Martin P, Busch D, Haenisch S, Müller J, et al. Dysregulation of mucosal membrane transporters and drug-metabolizing enzymes in ulcerative colitis. *J Pharm Sci* 2019; **108**:1035–46.
- Jahnel J, Fickert P, Hauer AC, Högenauer C, Avian A, Trauner M. Inflammatory bowel disease alters intestinal bile acid transporter expression. *Drug Metab Dispos* 2014; **42**:1423–31.

13. Lloret-Linares C, Miyauchi E, Luo HL, Labat L, Bouillot JL, Poitou C, et al. Oral morphine pharmacokinetic in obesity: the role of P-glycoprotein, MRP2, MRP3, UGT2B7, and CYP3A4 jejunal contents and obesity-associated biomarkers. *Mol Pharm* 2016;**13**:766–73.
14. Miyauchi E, Tachikawa M, Declèves X, Uchida Y, Bouillot JL, Poitou C, et al. Quantitative atlas of cytochrome P450, UDP-glucuronosyltransferase, and transporter proteins in jejunum of morbidly obese subjects. *Mol Pharm* 2016;**13**:2631–40.
15. Sugimoto R, Watanabe H, Ikegami K, Enoki Y, Imafuku T, Sakaguchi Y, et al. Down-regulation of ABCG2, a urate exporter, by parathyroid hormone enhances urate accumulation in secondary hyperparathyroidism. *Kidney Int* 2017;**91**:658–70.
16. Pan Y, Omori K, Ali I, Tachikawa M, Terasaki T, Brouwer KLR, et al. Altered expression of small intestinal drug transporters and hepatic metabolic enzymes in a mouse model of familial Alzheimer's disease. *Mol Pharm* 2018;**15**:4073–83.
17. Pote MS, Viswanathan G, Kesavan V. Increased intestinal folate absorption in experimental diabetes. *J Clin Biochem Nutr* 1998;**25**:25–30.
18. Said HM, Ghishan FK, Murrell JE. Intestinal transport of 5-methyltetrahydrofolate in streptozotocin-induced diabetes mellitus in the rat. *Diabetes Res* 1986;**3**:363–7.
19. Kamen BA, Smith AK. A review of folate receptor alpha cycling and 5-methyltetrahydrofolate accumulation with an emphasis on cell models. *in vitro. Adv Drug Deliv Rev* 2004;**56**:1085–97.
20. Qiu A, Jansen M, Sakaris A, Min SH, Chattopadhyay S, Tsai E, et al. Identification of an intestinal folate transporter and the molecular basis for hereditary folate malabsorption. *Cell* 2006;**127**:917–28.
21. Sarmento B, Martins S, Ferreira D, Souto EB. Oral insulin delivery by means of solid lipid nanoparticles. *Int J Nanomed* 2007;**2**:743–9.
22. Pan D, Das A, Liu D, Veazey RS, Pahar B. Isolation and characterization of intestinal epithelial cells from normal and SIV-infected rhesus macaques. *PLoS One* 2012;**7**:e30247.
23. Yang SJ, Lin FH, Tsai KC, Wei MF, Tsai HM, Wong JM, et al. Folic acid-conjugated chitosan nanoparticles enhanced protoporphyrin IX accumulation in colorectal cancer cells. *Bioconjugate Chem* 2010;**21**:679–89.
24. Diebold Y, Jarrín M, Sáez V, Carvalho ELS, Orea M, Calonge M, et al. Ocular drug delivery by liposome–chitosan nanoparticle complexes (LCS-NP). *Biomaterials* 2007;**28**:1553–64.
25. Jing LJ, Shao SM, Wang Y, Yang YB, Yue XL, Dai ZF. Hyaluronic acid modified hollow prussian blue nanoparticles loading 10-hydroxycamptothecin for targeting thermochemotherapy of cancer. *Theranostics* 2016;**6**:40–53.
26. Chen F, Goel S, Valdovinos HF, Luo H, Hernandez R, Barnhart TE, et al. *In vivo* integrity and biological fate of chelator-free zirconium-89-labeled mesoporous silica nanoparticles. *ACS Nano* 2015;**9**:7950–9.
27. Lin YH, Mi FL, Chen CT, Chang WC, Peng SF, Liang HF, et al. Preparation and characterization of nanoparticles shelled with chitosan for oral insulin delivery. *Biomacromolecules* 2007;**8**:146–52.
28. Furumiya M, Yamashiro T, Inoue K, Nishijima C, Ohta K, Hayashi Y, et al. Sustained inhibition of proton-coupled folate transporter by myricetin. *Drug Metabol Pharmacokin* 2015;**30**:154–9.
29. Yamashiro T, Ohta K, Inoue K, Furumiya M, Hayashi Y, Yuasa H. Kinetic and time-dependent features of sustained inhibitory effect of myricetin on folate transport by proton-coupled folate transporter. *Drug Metabol Pharmacokin* 2015;**30**:341–6.
30. Roger E, Lagarce F, Garcion E, Benoit JP. Lipid nanocarriers improve paclitaxel transport throughout human intestinal epithelial cells by using vesicle-mediated transcytosis. *J Controlled Release* 2009;**140**:174–81.
31. Jintapattanakit A, Junyaprasert VB, Kissel T. The role of mucoadhesion of trimethyl chitosan and PEGylated trimethyl chitosan nano-complexes in insulin uptake. *J Pharm Sci* 2010;**98**:4818–30.
32. Zhao RB, Diop-Bove N, Visentin M, Goldman ID. Mechanisms of membrane transport of folates into cells and across epithelia. *Annu Rev Nutr* 2011;**31**:177–201.
33. Alam C, Hoque MT, Finnell RH, Goldman ID, Bendayan R. Regulation of reduced folate carrier (RFC) by vitamin D receptor at the blood-brain barrier. *Mol Pharm* 2017;**14**:3848–58.
34. Boshnjaku V, Shim KW, Tsurubuchi T, Ichi S, Szany EV, Xi GF, et al. Nuclear localization of folate receptor alpha: a new role as a transcription factor. *Sci Rep* 2012;**2**:980.
35. Biabanikhankahdani R, Alitheen NBM, Ho KL, Tan WS. pH-Responsive virus-like nanoparticles with enhanced tumour-targeting ligands for cancer drug delivery. *Sci Rep* 2016;**6**:37891.
36. Jones SK, Sarkar A, Feldmann DP, Hoffmann P, Merkel OM. Revisiting the value of competition assays in folate receptor-mediated drug delivery. *Biomaterials* 2017;**138**:35–45.
37. Jin H, Pi J, Yang F, Jiang JH, Wang XP, Bai HH, et al. Folate-chitosan nanoparticles loaded with ursolic acid confer anti-breast cancer activities *in vitro* and *in vivo*. *Sci Rep* 2016;**6**:30782.
38. Zhou Y, Chen JH, Wang H, Wang CX, Zhang JY, Tao YW, et al. Synthesis and characterization of folate-poly(ethylene glycol) chitosan graft-polyethylenimine as a non-viral carrier for tumor-targeted gene delivery. *Afr J Biotechnol* 2011;**10**:6120–9.
39. Chanphai P, Konka V, Tajmir-Riahi HA. Folic acid–chitosan conjugation: a new drug delivery tool. *J Mol Liq* 2017;**238**:155–9.
40. Yang CX, Gao S, Kjemis J. Folic acid conjugated chitosan for targeted delivery of siRNA to activated macrophages *in vitro* and *in vivo*. *J Mater Chem B* 2014;**2**:8608–15.
41. Yamashiro T, Yasujima T, Ohta K, Inoue K, Yuasa H. Identification of the amino acid residue responsible for the myricetin sensitivity of human proton-coupled folate transporter. *Sci Rep* 2019;**9**:18105.
42. Peng SF, Tseng MT, Ho YC, Wei MC, Liao ZX, Sung HW. Mechanisms of cellular uptake and intracellular trafficking with chitosan/DNA/poly(γ -glutamic acid) complexes as a gene delivery vector. *Biomaterials* 2011;**32**:239–48.
43. Kaksonen M, Roux A. Mechanisms of clathrin-mediated endocytosis. *Nat Rev Mol Cell Biol* 2018;**19**:313–26.
44. Zhang XW, Qi JP, Lu Y, He W, Li XY, Wu W. Biotinylated liposomes as potential carriers for the oral delivery of insulin. *Nanomedicine* 2014;**10**:167–76.
45. He ZY, Santos JL, Tian HK, Huang HH, Hu YZ, Liu LX, et al. Scalable fabrication of size-controlled chitosan nanoparticles for oral delivery of insulin. *Biomaterials* 2017;**130**:28–41.
46. Shrestha N, Araújo F, Shahbazi MA, Mäkilä E, Gomes MJ, Herranz-Blanco B, et al. Drug delivery: thiolation and cell-penetrating peptide surface functionalization of porous silicon nanoparticles for oral delivery of insulin. *Adv Funct Mater* 2016;**26**:3374.
47. Yeh TH, Hsu LW, Tseng MT, Lee PL, Sonjae K, Ho YC, et al. Mechanism and consequence of chitosan-mediated reversible epithelial tight junction opening. *Biomaterials* 2011;**32**:6164–73.
48. Linz G, Djeljadini S, Steinbeck L, Köse G, Kiessling F, Wessling M. Cell barrier characterization in transwell inserts by electrical impedance spectroscopy. *Biosens Bioelectron* 2020;**165**:112345.
49. Bharali DJ, Lucey DW, Jayakumar H, Pudavar HE, Prasad PN. Folate-receptor-mediated delivery of InP quantum dots for bioimaging using confocal and two-photon microscopy. *J Am Chem Soc* 2005;**127**:11364–71.